J|A|C|S
A R T I C L E S

Design of Novel Inorganic−Organic Hybrid Materials Based on Iron-Chloranilate Mononuclear Complexes: Characteristics of Hydrogen-Bond-Supported Layers toward the Intercalation of Guests

Kunimitsu Nagayoshi,[†] Md. Khayrul Kabir,[†] Hiroshi Tobita,[‡] Kenji Honda,[‡]
Mitsuhiro Kawahara,[‡] Motomi Katada,[‡] Keiichi Adachi,[∥] Hiroyuki Nishikawa,[‡]
Isao Ikemoto,[‡] Hitoshi Kumagai,[§] Yuko Hosokoshi,[§] Katsuya Inoue,[§]
Susumu Kitagawa,[⊥] and Satoshi Kawata*,[∥]

*Contribution from the Department of Chemistry, Shizuoka University, Ohya, Shizuoka 422-8529,
Japan, Department of Chemistry, Graduate School of Scienec, Tokyo Metropolitan University,
Minami Ohsawa, Hachiouji, Tokyo 192-0397, Japan, Institute for Molecular Science, Myoudaiji,
Okazaki, Aichi 444-8585, Japan, Department of Chemistry, Graduate School of Science, Osaka
University, Machikaneyamacho Toyonaka, Osaka, 560-0043, Japan, and Department of Synthetic
Chemistry and Biological Chemistry, Graduate School of Engineering, Kyoto University,
Yoshida, Sakyo-ku, Kyoto 606-8501, Japan*

Received July 28, 2002

Abstract: Novel intercalation compounds constructed from the common two-dimensional hydrogen-bond-supported layers and functional guests $\{(H_{0.5}phz)_2[Fe(CA)_2(H_2O)_2]\cdot2H_2O\}_n$ (**1**), $\{[Fe(Cp)_2][Fe(CA)_2(H_2O)_2]\}_n$ (**2**), $\{[Fe(Cp^*)_2][Fe(CA)_2(H_2O)_2]\}_n$ (**3**), and $\{(TTF)_2[Fe(CA)_2(H_2O)_2]\}_n$ (**4**) (H_2CA = chloranilic acid, phz = phenazine, $[Fe(Cp)_2]$ = ferrocene, $[Fe(Cp^*)_2]$ = decamethylferrocene, TTF = tetrathiafulvalene) are described. The guest cations are introduced between the $\{[Fe(CA)_2(H_2O)_2]^{m-}\}_l$ layers by electrostatic (**1**−**4**) and $\pi-\pi$ stacking (**3**, **4**) interactions. $[Fe(Cp^*)_2]^+$ cations in **3** are stacked on each other making tilted columns which are included in the channel created by the chlorine atoms of CA^{2-} dianions. TTF cations in **4** are stacked face to face with two types of $S{\cdots}S$ distances (type A; 3.579(3) Å, and type B; 3.618(3) Å) making a columnar structure. The TTF cations in the stacked column have a head-to-tail arrangement with respect to the iron-chloranilate layer. Mössbauer spectroscopy suggests that $[Fe(CA)_2(H_2O)_2]^{m-}$ anion in **3** is consistent with high-spin ($S = 5/2$) iron(III) ions and $[Fe(Cp^*)_2]^+$ in the low-spin ($S = 1/2$) iron(III) ions. In **4**, Mössbauer spectroscopy shows high-spin iron(II) ions (IS = 1.10 mm·s^{-1} and QS = 1.66 mm·s^{-1} at 297 K) and high-spin iron(III) ions (IS = 0.42 mm·s^{-1} and QS = 1.27 mm·s^{-1} at 297 K), suggesting that the anionic layer of iron-chloranilate has a valence-trapped mixed-valence state. At the temperature range of 77−300 K, the compounds **1**, **2**, and **3** are EPR silent, whereas the EPR spectrum of **4** shows two types of signals with g = 2.008 indicating the radical form of TTF.

Introduction

The conventional synthetic scheme for intercalating guests into layered hosts entails a direct reaction of the guest with the host lattice.[1] Such heterogeneous reactions usually afford products with insufficient crystallinity. Through the incorporation of a guest species into a layered host, novel solids may be engineered with desired physical and chemical properties.[2] These materials may possess hybrid properties that have synergism of the properties shown by the host and the guest.[3] A particularly attractive feature of such layered hosts is that they serve as a template for the creation of intercalated supramolecular arrays.[4] The combination of two extremely different components, at the molecular level, provides an avenue to designing new nano-composite hybrid materials as well as the ability to modulate the properties of one or more of the components. In some circumstances, it is also a unique way to generate materials which have special properties that are not observed in the individual constituents.[5] It is expected that these properties can

* To whom correspondence should be addressed. Fax:+81-6-6850-5409.
E-mail: kawata@chem.sci.osaka-u.ac.jp.
† Shizuoka University.
‡ Tokyo Metropolitan University.
§ Institute for Molecular Science.
∥ Osaka University.
⊥ Kyoto University.

(1) Newman, S. P.; Jones, W. *New. J. Chem.* **1998**, 105.
(2) (a) Tseng, W.; Lin, J.; Mou, C.; Cheng, S.; Liu, S.; Chu, P. P.; Liu, H. *J. Am. Chem. Soc.* **1996**, *118*, 4411. (b) Müller, A.; Reuter, H.; Dillinger, S. *Angew. Chem., Int. Ed. Engl.* **1995**, *34*, 2328.

(3) (a) Ouahab, L. *Chem. Mater.* **1997**, *9*, 1909. (b) Kanatzidis, M. G.; Bissessur, R.; DeGroot, D. C.; Schindler, J. L.; Kannewurf, C. R. *Chem. Mater.* **1993**, *5*, 595.
(4) Mitzi, D. B. *J. Chem. Soc., Dalton Trans.* **2001**, 1.
(5) (a) Kondenkandath, T. A.; Lalena, J. N.; Zhou, W. L.; Carpenter, E. E.; Sangregorio, C.; Falster, A. U.; Simmons, W. B., Jr.; O'Connor, C. J.; Wiley, J. B. *J. Am. Chem. Soc.* **1999**, *121*, 10743. (b) Tolbert, S. H.; Sieger, P.; Stucky, G. D.; Aubin, S. M. J.; Wu, C.; Hendrickson, D. N. *J. Am. Chem. Soc.* **1997**, *119*, 8652.
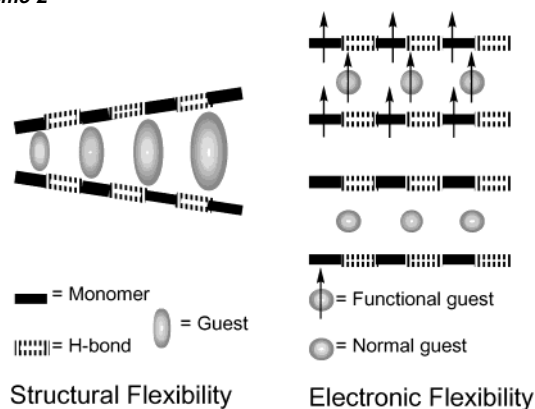
Scheme 1

Scheme 2
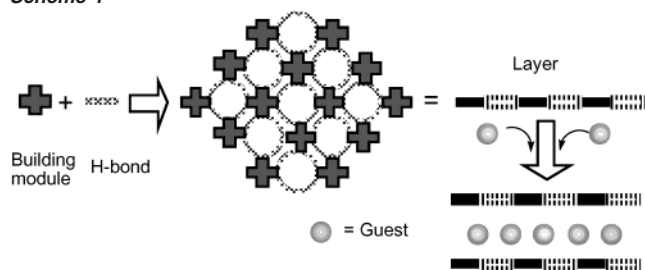
be enhanced or fine-tuned through the coupling between organic and inorganic domains.

Fabrication of inorganic−organic hybrid materials is typically based on a modular approach, where discrete building blocks are linked into larger networks.[6] Considerable effort has been focused on the supramolecular networks assembled by covalent bonding,[7] coordination bonding,[8] hydrogen bonding,[9] or other molecular interactions.[10] Our strategy to control molecular packing in crystalline materials uses strong hydrogen bonds in combination with metal−ligand bonds (Scheme 1). This approach provides a means to control the rigidity of a supramolecular framework of molecules joined by metal−ligand interactions by selective incorporation of more flexible hydrogen bonds between molecules. This method should produce a large single crystal since hydrogen-bonded structures form reversibly and exhibit slower kinetics for nucleation and growth of crystal than coordination polymers. Moreover, this strategy combines the rich structural and physical chemistry of transition metals with organic compounds to create crystalline materials with potential for optical and microporous applications.

Dihydroxybenzoquinone derivatives have frontier orbitals with energies comparable to those of the transition-metal ions and the nature of the reduced and oxidized species depends on the metal ions and the coordination environment.[11] Examples from this class of compounds include $[M_2(CTH)_2(DHBQ)]^{3+}$ (M = Cr(III) or Fe(III); CTH = *dl*-5,7,7,12,14,14-hexamethyl-1,4,8,11-tetraazacyclotetradecane; H_2DHBQ = dihydroxybenzoquinone $(C_6H_4O_4)$)[12] and $(Bu_4N)_2[Mo_4O_{10}(DHBQ)_2]$.[13] The existence of the compound $[M_2(CTH)_2(DHBQ)]^{3+}$ demonstrated that radical species can be stabilized with iron and chromium. The DHBQ radical behaves as a linking ligand, which can yield reasonably strong antiferromagnetic coupling with the metals. Moreover, a mixed valence iron coordination polymer with DHBQ was obtained by solid-state I_2 oxidation.[14] The back-

ground of this chemistry prompts us to construct new layer compounds by using redox active metals such as iron and DHBQ derivatives.

Previously, we reported structural characterization of two-dimensional layered structures constructed from metal-chloranilate mononuclear complexes $[M(CA)_2(H_2O)_2]^{2-}$ (M = Cu(II) or Co(II)) by hydrogen-bonding interaction.[15] The layers $\{[M(CA)_2(H_2O)_2]^{2-}\}_1$ intercalate 4-hydroxypyridinium (4-pyOH$_2^+$) and 3-hydroxypyridinium (3-pyOH$_2^+$)[15a] by hydrogen-bonding interaction and electrostatic interaction, and $\{[Fe(CA)_2(H_2O)_2]^{m-}\}_1$ intercalate phenazinium cation $([H_{0.5}phz]^{0.5+})$ $(\{(H_{0.5}phz)_2[Fe(CA)_2(H_2O)_2]\cdot 2H_2O\}_n)$ (**1**)[15b] and ferrocenium cation $([Fe(Cp)_2]^+)$ $(\{[Fe(Cp)_2][Fe(CA)_2(H_2O)_2]\}_n$ (**2**))[15c] only by the electrostatic interaction. The extension of this chemistry would afford new hydrogen-bonding assemblies if the layered compounds are constructed using the similar building blocks and charged guests with functionalities such as conducting or photosensitized properties.

To take advantage of the anionic complex $[Fe(CA)_2(H_2O)_2]^{m-}$ as a hydrogen-bonding module, it is attempted to intercalate the metallocenium and TTF donor derivatives as the functional cationic guests, which are well-known in charge-transfer materials and exhibit particular physical properties such as electrical conductivity and magnetism. Novel intercalation compounds constructed from the common two-dimensional hydrogen-bond-supported layers and functional guests $\{[Fe(Cp*)_2][Fe(CA)_2(H_2O)_2]\}_n$ (**3**) and $\{(TTF)_2[Fe(CA)_2(H_2O)_2]\}_n$ (**4**) $([Fe(Cp*)_2]$ = decamethylferrocene; TTF = tetrathiafulvalene) are described. The guest cations are introduced between the $\{[Fe(CA)_2(H_2O)_2]^{m-}\}_1$ layers by the electrostatic interaction. The $\{[Fe(CA)_2(H_2O)_2]^{m-}\}_1$ layers are so flexible that they are able to tune their charge distribution and interlayer distances to accommodate guests of various sizes and electronic states (Scheme 2). Compound **4** is a rare example of hydrogen-bonded layer of monomeric complexes, which shows electronic flexibility toward the intercalation of charged guests.

In this paper, the relationships between the host structure of iron-chloranilate layers and the intercalated charged guests are

(6) (a) Aakeröy, C. B.; Beatty, A. M.; Leinen, D. S.; Lorimer, K. R. *Chem. Commun.* **2000**, 935. (b) Abrahams, B. F.; Batten, S. R.; Hamit, H.; Hoskins, B. F.; Robson, R. *Angew. Chem., Int. Ed. Engl.* **1996**, *35*, 1690.
(7) (a) Batten, S. R.; Robson, R. *Angew. Chem., Int. Ed. Engl.* **1998**, *37*, 1460. (b) Power, K. N.; Hennigar, T. L.; Zaworotko, M. J. *Chem. Commun.* **1998**, 595. (c) Yagi, O. M.; Li, G.; Li, H. *Nature* **1995**, *378*, 703.
(8) (a) Holliday, B. J.; Mirkin, C. A. *Angew. Chem., Int. Ed.* **2001**, *40*, 2022. (b) Fujita, M.; Umemoto, K.; Yoshizawa, M.; Fujita, N.; Kusukawa, T.; Biradha, K. *Chem. Commun.* **2001**, 509. (c) Kabir, M. K.; Kawahara, M.; Kumagai, H.; Adachi, K.; Kawata, S.; Ishii, T.; Kitagawa, S. *Polyhedron* **2001**, *20*, 1417.
(9) (a) Bernhardt, P. V. *Inorg. Chem.* **1999**, *38*, 3481. (b) Chowdhry, M. M.; Mingos, D. M. P.; White, A. J. P.; Williams, D. J. *Chem. Commun.* **1996**, 899. (c) Qin, Z.; Jennings, M. C.; Puddephatt, R. J. *Inorg. Chem.* **2001**, *40*, 6220.
(10) Zheng, S.-L.; Tong, M.-L.; Fu, R.-W.; Chen, X.-M.; Ng, S.-W. *Inorg. Chem.* **2001**, *40*, 3562.
(11) (a) Kawata, S.; Kitagawa, S. *Coord. Chem. Rev.* **2002**, *224*, 11. (b) Masui, H.; Freda, A. L.; Zerner, M. C.; Lever, A. B. P. *Inorg. Chem.* **2000**, *39*, 141. (c) Ward, M. D.; McCleverty, J. A. *J. Chem. Soc., Dalton Trans.* **2002**, 275.
(12) Dei, A.; Gatteschi, D.; Pardi, L.; Russo, U. *Inorg. Chem.* **1991**, *30*, 2589.
(13) Liu, S.; Shaikh, S. N.; Zubieta, J. *Inorg. Chem.* **1989**, *28*, 723.

(14) (a) Wrobleski, J. T.; Brown, D. B. *Inorg. Chem.* **1979**, *18*, 2738. (b) Kawata, S.; Kitagawa, S.; Kumagai, H.; Ishiyama, T.; Honda, K.; Tobita, H.; Adachi, K.; Katada, M. *Chem. Mater.* **1998**, *10*, 3902.
(15) (a) Kawata, S.; Kumagai, H.; Adachi, K.; Kitagawa, S. *J. Chem. Soc., Dalton Trans.* **2000**, 2409. (b) Kabir, M. K.; Kawata, S.; Adachi, K.; Tobita, H.; Miyazaki, N.; Kumagai, H.; Katada, M.; Kitagawa, S. *Mol. Cryst. Liq. Cryst.* **2000**, *341*, 491. (c) Kawata, S.; Kumagai, H.; Kitagawa, S.; Honda, K.; Enomoto, M.; Katada, M. *Mol. Cryst. Liq. Cryst.* **1996**, *286*, 51. (d) Kabir, M. K.; Miyazaki, N.; Kawata, S.; Adachi, K.; Kumagai, H.; Inoue, K.; Kitagawa, S.; Iijima, K. *Coord. Chem. Rev.* **2000**, *198*, 157−169.

discussed. In addition to the investigation of the structure and physical properties of **3** and **4**, these aspects are also investigated in **1** and **2**.

Experimental Section

Syntheses. {($H_{0.5}$phz)$_2$[Fe(CA)$_2$(H$_2$O)$_2$]·2H$_2$O}$_n$ **(1).** The compound was prepared according to the literature procedure previously reported.[15b] Yield; 70%. Calcd for FeCl$_4$O$_{12}$N$_4$C$_{36}$H$_{24}$: C, 47.92; H, 2.68; N, 6.19%. Found: C, 47.80; H, 2.71; N, 6.22%.

{[Fe(Cp)$_2$][Fe(CA)$_2$(H$_2$O)$_2$]}$_n$ **(2).** The compound was prepared according to the literature procedure previously reported.[15c] Yield; 40%. Calcd for Fe$_2$Cl$_4$O$_{10}$C$_{22}$H$_{34}$: C, 38.19; H, 2.04%. Found: C, 38.47; H, 2.16%.

{[Fe(Cp*)$_2$][Fe(CA)$_2$(H$_2$O)$_2$]}$_n$ **(3).** An aqueous solution (1 mL) of iron(III) nitrate nonahydrate (5 mmol·l^{-1}) was transferred to a glass tube, then an ethanol-acetonitrile mixture (2 mL) of chloranilic acid (10 mmol·l^{-1}) and Fe(Cp*)$_2$ (5 mmol·l^{-1}) was poured into the glass tube without mixing the two solutions. Dark purple crystals began to form at ambient temperature in 2 months. One of these crystals was used for X-ray crystallography. Physical measurements were conducted on a polycrystalline powder that was synthesized as follows: an aqueous solution (1000 mL) of iron(III) nitrate nonahydrate (5 mmol·l^{-1}) was added to an ethanol-acetonitrile mixture (2000 mL) of chloranilic acid (10 mmol·l^{-1}) and Fe(Cp*)$_2$ (5 mmol·l^{-1}). Upon stirring the mixture, dark purple powders appeared in one month. Yield; 40%. Calcd for Fe$_2$Cl$_4$O$_{10}$C$_{32}$H$_{34}$: C, 46.19; H, 4.12%. Found: C, 46.16; H, 4.07%.

{(TTF)$_2$[Fe(CA)$_2$(H$_2$O)$_2$]}$_n$ **(4).** An aqueous solution (1 mL) of iron-(II) tetrafluoroborate (12 mmol·l^{-1}) was transferred to a glass tube, then an acetonitrile-water (4:1) mixture (1 mL) of (TTF)$_3$(BF$_4$)$_2$ (4.5 mmol·l^{-1}) and an acetonitrile solution (1 mL) of chloranilic acid (18 mmol·l^{-1}) were poured into the tube without mixing the three solutions under nitrogen atmosphere. Black crystals began to form at ambient temperature in 3 weeks. One of these crystals was used for X-ray crystallography. Physical measurements were conducted on a poly-crystalline powder that was synthesized as follows: an aqueous solution (500 mL) of iron(II) tetrafluoroborate (12 mmol·l^{-1}) was added to an acetonitrile-water (4:1) mixture (500 mL) of (TTF)$_3$(BF$_4$)$_2$ (4.5 mmol l^{-1}) and an acetonitrile solution (500 mL) of chloranilic acid (18 mmol·l^{-1}). Upon stirring of the mixture, black powders appeared immediately. Yield; 60%. Calcd for Fe$_1$Cl$_4$S$_8$O$_{10}$C$_{24}$H$_{12}$: C, 31.52; H, 1.32%. Found: C, 31.54; H, 1.34%.

Powder XRD. Identity of the batches for physical measurements and single-crystal data collection was established by comparison of the powder X-ray diffraction patterns (XRD). The XRD patterns (supplementary figures, S1, S2, S3, and S4) of the powder samples are in good agreement with the simulated patterns reproduced from the Fc values of the calculated crystal structures.

Physical Measurements. IR spectra of KBr disks were measured with a JASCO FT/IR-410 spectrophotometer. UV and visible spectra were measured on KBr disks of powder sample with a JASCO V-570 spectrophotometer. EPR measurements were performed over the range 77−300 K with an X-band spectrometer Bruker ESP-300 operating at 9.1−9.9 GHz. The ^{57}Fe Mössbauer spectra were obtained by using an Wissel Mössbauer spectrometer with a proportional counter. A ^{57}Co(Rh) source moving in a constant acceleration mode was used for the measurements. The velocity scale was calibrated by using a metallic iron-foil spectrum. The isomer shift (*IS*) and quadrupole splitting (*QS*) were obtained by least-squares fitting of the Mössbauer data to Lorentzian line shapes. Magnetic susceptibility data were recorded over the temperature range from 2 to 300 K in the presence of a magnetic field between 50 and 5000 G with a SQUID susceptometer (Quantum Design, San Diego, CA). All data were corrected for diamagnetism which was calculated from Pascal's table.[16] X-ray powder diffraction data were collected on a Rigaku RINT 2000 diffractometer by using

(16) Kahn, O. *Molecular Magnetism*; VCH Publishers Inc.: New York, 1993.

Table 1. Crystallographic Data for **3** and **4**

compound	3	4
formula	Fe$_2$Cl$_4$C$_{32}$O$_{10}$H$_{34}$	FeCl$_4$S$_8$O$_{10}$C$_{24}$H$_{12}$
molecular weight	832.12	914.55
crystal system	triclinic	monoclinic
space group	P$\bar{1}$ (no. 2)	C2/m (no. 12)
crystal color	dark purple	black
a/Å	9.320(1)	7.184(5)
b/Å	13.228(2)	17.077(6)
c/Å	7.333(2)	13.744(4)
α/°	97.08(2)	90
β/°	112.90(1)	100.56(4)
γ/°	86.50(1)	90
V (Å^3)	826.4(3)	1657(1)
Z	1	2
D_{calc} (g/cm^3)	1.672	1.832
F(000)	852.00	916.00
μ(Mo Kα)(cm^{-1})	12.73	13.34
diffractometer	AFC7R	AFC7R
temp (K)	296.0	296.0
2θmax (deg)	55.0	55.0
refines collcd	4106	2120
unique reflcns	3805	2089
no. of obsd reflcns	2774 ($I > 2\sigma$)	1250 ($I > 2\sigma$)
no. of variables	221	113
R	0.041	0.036
R_w	0.122	0.101
GOF	1.02	1.01

Cu(Kα) radiation. Laser Raman spectra were recorded with Ar$^+$ ion excitation using a JASCO R-600 spectrometer. The resistivity of the samples was measured by the conventional four-probe method in the temperature range 130−300 K.

Crystallographic Data Collection and Refinement of the Structure. A suitable crystal was chosen and mounted on a glass fiber with epoxy resin. Data collection was carried out on a Rigaku AFC7R with graphite-monochromated Mo(Kα) radiation ($\lambda = 0.71069$ Å). Cell constants and orientation matrix for intensity data collection for each crystal were based on the setting angles of 25 carefully centered reflections in the ranges 28.4° < 2θ < 30.0° for **3** and 25.1° < 2θ < 29.1° for **4**. Crystallographic data are given in Table 1. The structures were solved by direct methods (Rigaku TEXSAN crystallographic software package of Molecular Structure Corporation). Full-matrix least-squares refinements (SHELXL-97)[17] were carried out with anisotoropic thermal parameters for all non-hydrogen atoms. All the hydrogen atoms for **3** were placed in the calculated positions and not refined. All the hydrogen atoms for **4** were located in the Fourier difference maps and refined isotropically. Atomic coordinates are given in the supplementary data (Table S1).

Results and Discussion

Crystal Structures. {[Fe(Cp*)$_2$][Fe(CA)$_2$(H$_2$O)$_2$]}$_n$ (3). The structure of compound **3** consists of two mononuclear units, [Fe(CA)$_2$(H$_2$O)$_2$]$^-$ anion and [Fe(Cp*)$_2$]$^+$ cation. An ORTEP[18] drawing of the structure around the iron ions with the atom numbering scheme is shown in Figure 1a. The iron atoms sit on the crystallographic inversion centers. The selected bond distances and angles with their estimated standard deviations are listed in Table 2. The geometry around Fe(1) of [Fe(CA)$_2$(H$_2$O)$_2$]$^-$ anion is an elongated octahedron involving the four oxygen atoms of two CA^{2-} anions in the equatorial position (1.992(2) Å, Fe(1)−O(1), Fe(1)−O(1′); 1.998(2) Å, Fe(1)−O(2), Fe(1)−O(2′)) and two water molecules in the axial position (2.050(3)

(17) Sheldrick, G. M. *SHELEX-97 Program for X-ray Crystal Structure Refinement*; University of Göttingen: Göttingen, Germany, 1997.
(18) Johnson, C. K. *ORTEP*; Report ORNL-5138, Oak Ridge National Laboratory: Oak Ridge, TN, 1976.
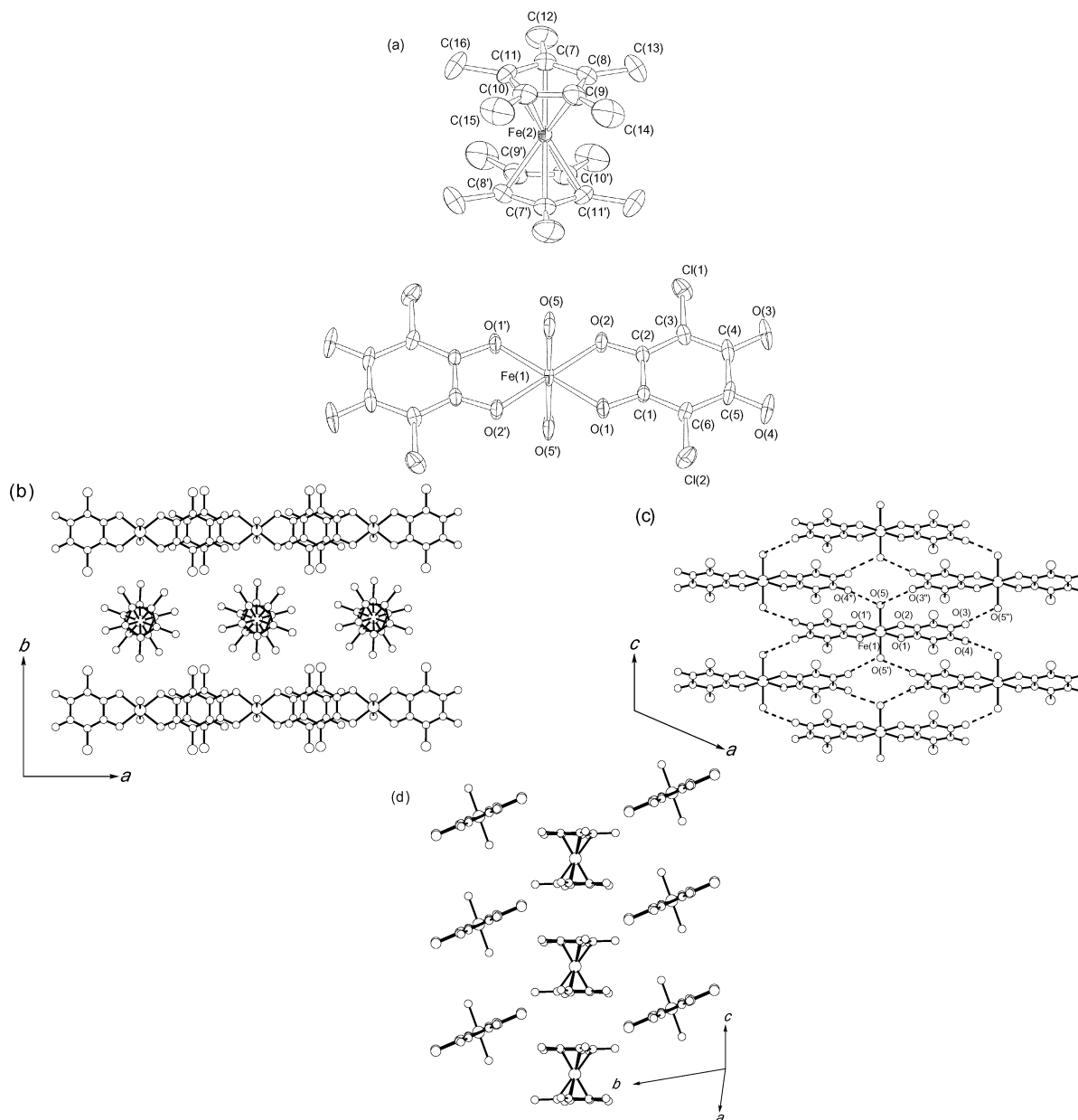
Figure 1. Crystal structure of **3**; (a) ORTEP drawing of a mononuclear unit with labeling scheme (thermal ellipsoids at the 50% probability level for Fe, Cl, O, and C atoms). Spheres of the hydrogen atoms have been arbitrarily reduced. (b) assembled structure along the *c*-axis, (c) sheet structure of {[Fe-(CA)$_2$(H$_2$O)$_2$]$^-$}$_l$, (the dashed lines denote hydrogen bonds), and (d) columnar structure of [Fe(Cp*)$_2$]$^+$ cations.

Å, Fe(1)−O(5), Fe(1)−O(5′)). The Fe(1)−O bond distances are similar to those of **1** and **2**, which indicates that the oxidation state of Fe(1) is 3+. The symmetrical coordination of the CA^{2-} dianion is recognized from the similar C−O distances 1.286(3) Å (C(1)−O(1)), 1.284(4) Å (C(2)−O(2)) for coordinated and 1.238(4) Å (C(4)−O(3)), 1.233(4) Å (C(5)−O(4)) for uncoordinated oxygen atoms. These bond distances suggest that CA^{2-} dianion is in the *o*-quinone form, where C−O bonds of equal length are located in *ortho* position.[11a,15a,19] The coordination geometry around Fe(2) of [Fe(Cp*)$_2$]$^+$ cation shows near D_{5d} symmetry, consisting of two Cp*$^-$ (pentamethylcyclopentadienyl) anions. The Fe(2)−C, C−C, and C−Me distances range from 2.081(3) to 2.097(4) Å, from 1.411(6) to 1.434(5) Å, and from 1.496(6) to 1.510(6) Å, respectively. The Fe(2)−C bond

distance of **3** is slightly shorter than that of the neutral Cp*.[20] However, the C−C and C−Me distances remain the same.

The crystal packing structure of **3** is shown in Figure 1, which consists of a two-dimensional layer of [Fe(CA)$_2$(H$_2$O)$_2$]$^-$ anions with [Fe(Cp*)$_2$]$^+$ cations intercalated in between. [Fe(CA)$_2$-(H$_2$O)$_2$]$^-$ anions in **3** make a two-dimensional layer supported by both the hydrogen-bonding interaction and the stacking interaction extending to the *ac*-plane. There are two types of hydrogen bonds that occur between the coordinated water and the terminal oxygen atoms of CA^{2-}, (O(5)−O(3″); 2.686(3) Å, O(5)−O(4*); 2.678(4) Å), on the nearest-neighbor anionic monomers. Adjacent monomers are stacked on each other with coordinated chloranilate plane to support the layers: the distance

(19) Abrahams, B. F.; Hoskins, B. F.; Robson, R. *Acta Crystallogr.* **1996**, *C52*, 2766.

(20) (a) Struchkov, Y. T.; Andrianov, V. G.; Sal'Nikova, T. N.; Lyatifov, I. R.; Materikova, R. B. *J. Organomet. Chem.* **1978**, *145*, 213. (b) Freyberg, D. P.; Robbins, J. L.; Raymond, K. N.; Smart, J. C. *J. Am. Chem. Soc.* **1979**, *101*, 892.

Table 2. Selected Bond Distances (Å) and Angles (°)

3			
Fe(1)−O(1)	1.992(2)	Fe(1)−O(2)	1.998(2)
Fe(1)−O(5)	2.050(3)	Cl(1)−C(3)	1.719(3)
Cl(2)−C(6)	1.714(3)	O(1)−C(1)	1.286(3)
O(2)−C(2)	1.284(4)	O(3)−C(4)	1.238(4)
O(4)−C(5)	1.233(4)	C(1)−C(2)	1.508(4)
C(1)−C(6)	1.377(4)	C(2)−C(3)	1.377(4)
C(3)−C(4)	1.417(4)	C(4)−C(5)	1.542(5)
C(5)−C(6)	1.435(4)	Fe(2)−C(7)	2.093(4)
Fe(2)−C(8)	2.081(3)	Fe(2)−C(9)	2.089(3)
Fe(2)−C(10)	2.097(4)	Fe(2)−C(11)	2.093(5)
O(1)−Fe−O(2′)	99.24(9)	O(1)−Fe−O(2)	80.76(9)
O(1)−Fe−O(5)	89.4(1)	Fe(1)−O(1)−C(1)	114.9(2)
Fe(1)−O(2)−C(2)	114.8(2)	O(1)−C(1)−C(2)	114.8(2)
O(1)−C(1)−C(6)	124.5(3)	C(2)−C(1)−C(6)	120.7(2)
O(2)−C(2)−C(1)	114.7(2)	O(2)−C(2)−C(3)	125.1(2)
C(1)−C(2)−C(3)	120.2(2)	Cl(1)−C(3)−C(2)	120.0(2)
Cl(1)−C(3)−C(4)	118.8(2)	C(2)−C(3)−C(4)	121.2(2)
O(3)−C(4)−C(3)	123.6(3)	O(3)−C(4)−C(5)	117.4(3)
C(3)−C(4)−C(5)	119.0(2)	O(4)−C(5)−C(4)	118.8(3)
Cl(2)−C(6)−C(1)	120.6(2)	Cl(2)−C(6)−C(5)	118.5(2)
C(1)−C(6)−C(5)	120.8(3)		

4			
Fe−O(1)	2.053(2)	Fe−O(3)	2.063(4)
Cl−C(3)	1.725(3)	O(1)−C(1)	1.274(3)
O(2)−C(3)	1.238(4)	C(1)−C(1′)	1.514(6)
C(1)−C(2)	1.383(4)	C(2)−C(3)	1.414(4)
C(3)−C(3′)	1.542(6)	S(1)−C(4)	1.725(3)
S(1)−C(6)	1.731(4)	S(2)−C(5)	1.728(3)
S(2)−C(7)	1.725(4)	C(4)−C(5)	1.373(7)
C(6)−C(6′)	1.313(8)	C(7)−C(7′)	1.320(8)
O(1)−Fe−O(1′)	78.4(1)	Fe−O(1)−C(1)	115.7(2)
O(1)−Fe−O(1*)	101.6(1)	Cl−C(2)−C(1)	120.2(2)
Cl−C(2)−C(3)	118.7(2)	O(1)−C(1)−C(1′)	115.1(2)
O(1)−C(1)−C(2)	124.8(2)	C(1′)−C(1)−C(2)	120.1(2)
C(1)−C(2)−C(3)	121.1(3)	O(2)−C(3)−C(2)	123.8(3)
O(2)−C(3)−C(3′)	117.5(2)	C(2)−C(3)−C(3′)	118.7(2)
C(4)−S(1)−C(6)	95.1(2)	C(5)−S(2)−C(7)	95.2(2)
S(1)−C(4)−S(1′)	114.9(3)	S(1)−C(4)−C(5)	122.6(1)
S(2)−C(5)−S(2′)	114.7(3)	S(2)−C(5)−C(4)	122.7(1)

of the nearest-neighbor C−C is 3.438(5) Å. The chlorine atoms of CA^{2-} project forward to the outside of the layer creating channels along the c-direction. The $[Fe(Cp^*)_2]^+$ cations are included in the channel. $[Fe(Cp^*)_2]^+$ cations are stacked on each other by Cp* rings along the c-axis to form a one-dimensional columnar structure in the channel (nearest-neighbor C−C distance: 3.929(6) Å), and the distance of the nearest-neighbor Fe(2)−Fe(2′) is 7.333(2) Å. This columnar structure of **3** is close to that of $\{[Fe(Cp^*)_2][C_3(C(CN)_3)_3]\}_n$,[21] where the distances of the nearest-neighbor intermolecular C−C and Fe−Fe are 3.91 and 7.29 Å, respectively, but are different from those of $\{[Fe(Cp^*)_2]_4[SiMo_{12}O_{40}](DMF)\}_n$.[22] In the latter case, the $[Fe(Cp^*)_2]^+$ cations are not stacked in the straight way but rather tilted with each other and form the zigzag chain structure. The one-dimensional straight columnar structure of $[Fe(Cp^*)_2]^+$ cation is very rare. This structural feature is reflected on its magnetic property (vide infra).

$\{(TTF)_2[Fe(CA)_2(H_2O)_2]\}_n$. (4) The structure of compound **4** consists of a mononuclear anion of iron-chloranilate complex similar to **3** and two TTF cations. An ORTEP drawing of **4** is shown in Figure 2a. The iron atom sits on the crystallographic inversion center. The selected bond distances and angles with

their estimated standard deviations are listed in Table 2. The geometry around the iron ion is an elongated octahedron involving the four oxygen atoms of two CA^{2-} anions in the equatorial position (Fe−O(1); 2.053(2) Å) and two oxygen atoms of two water molecules in the axial position (Fe−O(3); 2.063(2) Å). The Fe−O(CA^{2-}) bond distances of **4** are shorter than those of $\{[Fe(II)(CA)(H_2O)_2](G)\}_n$ (Fe(II)−O(CA^{2-}); 2.14 Å)[14b] and longer than those of **1**, **2**, and **3** (mean Fe(III)−O; 1.99 Å). In compound **4**, however, the Fe−O(H_2O) axial bond distance and the symmetrical coordination of CA^{2-} with their o-quinone form (1.274(3) Å (C(1)−O(1)) for coordinated and 1.238(4) Å (C(3)−O(2)) for uncoordinated oxygen atoms) are similar to that of **1**, **2**, and **3**. The primary assumption which is extracted from these features is that the oxidation state of iron ion in **4** is between 2+ and 3+, that is, mixed-valence state.

The crystal packing structure of **4** is shown in Figure 2, which consists of a two-dimensional layer of mononuclear iron-chloranilate complexes with TTF cations intercalated in between. Each monomer in the layer is connected to the four nearest neighbors making rhombic arrangement by four hydrogen bonds of 2.678(3) Å, formed between the coordinated water molecules and the two free oxygen atoms on each terminal chloranilate group. The layers spread along the ab plane. The chloranilate planes of the nearest-neighbor monomers are also stacked face to face: the nearest-neighbor C−C distance is 3.559(5) Å. The hydrogen-bonding mode and the bond strength in the layers of **3** and **4** are very similar to each other. The common feature that provides the similar layer structures is induced by the coordination of two water molecules in the trans positions of octahedral monomers allowing the chloranilate planes to remain in the same plane.

The TTF cations are intercalated between the layers by the electrostatic interaction, making the columnar array along the a-direction. The TTF cations in the stacked column of **4** have a head-to-tail arrangement with respect to the iron-chloranilate layer. Within the columnar array of TTF cations, there is nominally ring-over-bond type molecular overlap. TTF cations are stacked face to face with two types of S···S distances (type A; 3.579(3) Å, and type B; 3.618(3) Å). The mean stacking distance observed here is larger than that of dimeric TTF cations 3.20−3.40 Å[23] and almost the same in other columnar arrays 3.50−3.60 Å,[24] indicating that the stacking interaction between TTF cations in the column is weaker than those in dimeric units.

On the other hand, the estimated charge of iron ion (2+ < n < 3+) indicates that the charge on TTF is intermediate between 0.5+ and 1+. Moreover, it is also possible to calculate the charge from the C=C and C−S bond distances in TTF cation.[23a,25] In Table 3, bond distances and estimated charge of TTF in **4** are compared with corresponding distances and charges found in other compounds. According to the bond distances, the charge is estimated to 0.7+ for TTF in **4**. Thus, the oxidation

(21) Miller, J. S.; Zhang, J. H.; Reiff, W. M. *Inorg. Chem.* **1987**, *26*, 600.
(22) Maguerés, P. L.; Ouahab, L.; Golhen, S.; Grandjean, D.; Peña, O.; Jegaden, J.-C.; Gómez-Garcia, C. J.; Delhaés, P. *Inorg. Chem.* **1994**, *33*, 5180.
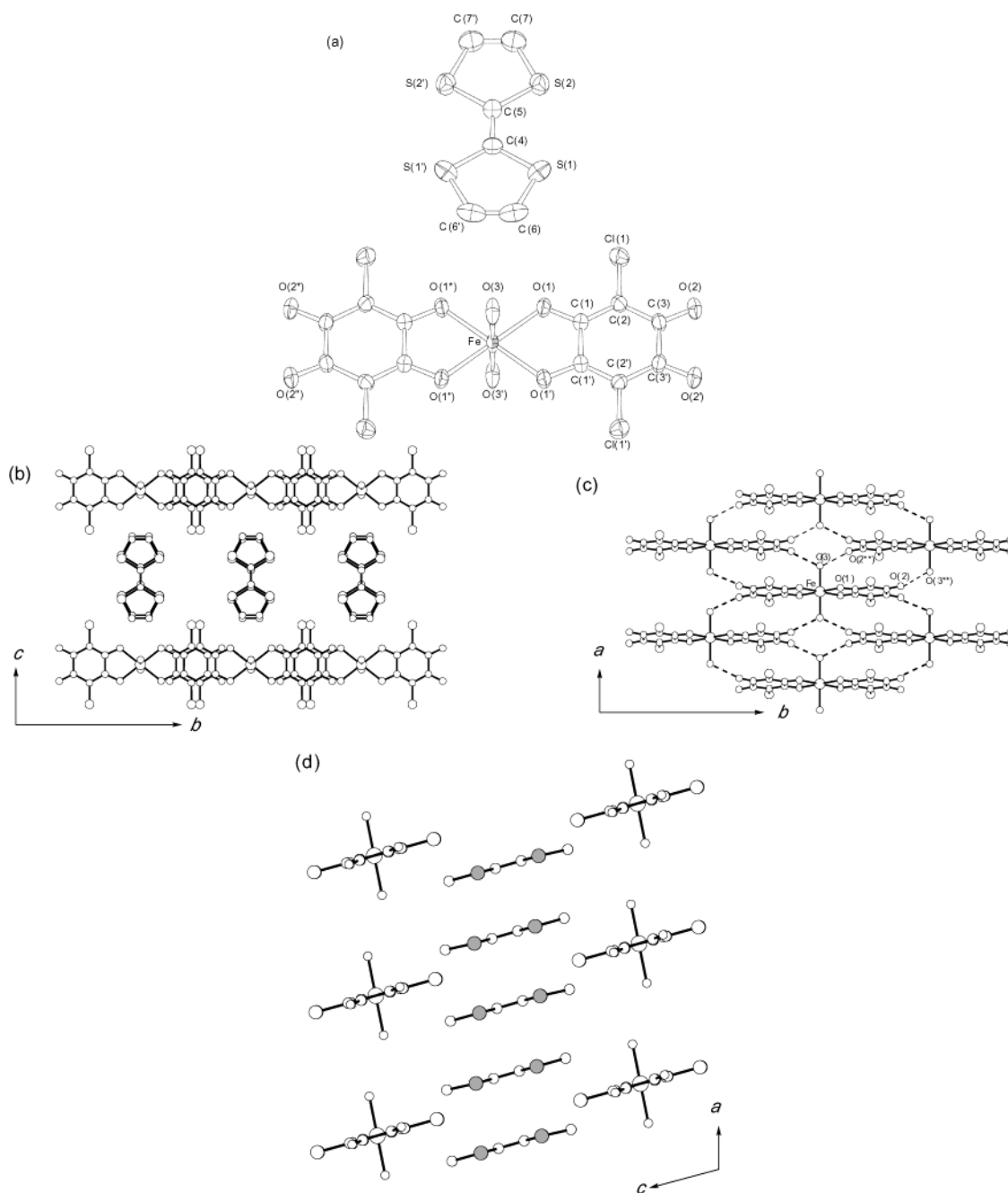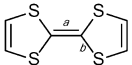
(23) (a) Coronado, E.; Galán-Mascarós, J. R.; Gómez-García, C. J. *J. Chem. Soc., Dalton. Trans.* **2000**, 205. (b) Clemente-León, M.; Coronado, E.; Galán-Mascarós, J. R.; Gómez-García, C. J.; Candell, E. *Inorg. Chem.* **2000**, *39*, 5394.
(24) (a) Ouahab, L.; Bencharif, M.; Mhanni, A.; Pelloquin, D.; Halet, J. F.; Peña, O.; Padiou, J.; Grandjean, D. *Chem. Mater.* **1992**, *4*, 666. (b) LaPlaca, S. J.; Corfield, P. W. R.; Thomas, R.; Scott, B. A. *Solid State Commun.* **1975**, *17*, 635. (c) Kistenmacher, T. J.; Rossi, M.; Chiang, C. C.; Duyne, R. P. V.; Seiedle, A. R. *Inorg. Chem.* **1980**, *9*, 3604.
(25) Umland, T. C.; Allie, S.; Kuhlmann, T.; Coppens, P. *J. Phys. Chem.* **1988**, *92*, 6456.

Figure 2. Crystal structure of **4**; (a) ORTEP drawing of a mononuclear unit of compound **4** with labeling scheme (thermal ellipsoids at the 50% probability level for Fe, S, Cl, O, and C atoms). Spheres of the hydrogen atoms have been arbitrarily reduced. (b) assembled structure along the *a*-axis, (c) sheet structure of $\{[Fe(CA)_2(H_2O)_2]^{m-}\}_l$, (the dashed lines denote hydrogen bonds), and (d) columnar structure of TTF cations.

state of the iron ion in **4** is between 2+ and 3+ and reflected in Mössbauer spectra and magnetic susceptibility (vide infra).

Flexibility of Anionic Layer $\{[Fe(CA)_2(H_2O)_2]^{m-}\}_l$. Iron-chloranilate intercalation compounds have been synthesized with different guests. A common feature of the compounds of **1**, **2**, **3**, and **4** is that the guests are intercalated between the layers fabricated from the iron-chloranilate mononuclear complexes. The chloranilate-containing layers have a rhombic arrangement of $[Fe(CA)_2(H_2O)_2]^{m-}$ anions which connect the four nearest-neighbor monomers with the same type of stacking interaction and hydrogen-bonding interaction. The guests are intercalated in the channels between the anionic layers, created by the chlorine atoms of CA^{2-}. The cations are introduced and stabilized by electrostatic and stacking interactions and form

the one-dimensional columnar structure in the channel. This structural feature is different from those of $\{(G)_2[M(CA)_2-(H_2O)_2]\}_n$ (M = Cu^{2+}, Co^{2+}).[15a] The layered arrangement of these compounds is distorted, which is induced by the electronic configuration of the metal ions and the strong hydrogen-bonding interactions between the layers and the guests.

Interestingly, slight differences are observed in the assembled structure of **1**–**4** constructed from the common anionic layer, (Table 4). These changes are caused by the intercalation of different types of guests that ultimately affect the crystal packing structure. The main difference resides in the interlayer distances (Fe(1)−Fe(1″)) 14.57 Å (**1**), 9.79 Å (**2**), 13.13 Å (**3**), and 13.45 Å (**4**) (Scheme 3). The arrangement of monomers also affects the layer structures. Especially, the variation is clearly observed

Table 3. Comparison of Mean Bond Lengths a and b, Bond Distances Ratio r, and Estimated Formal Charge (Q) for TTF

compound	a/Å	b/Å	$r = a/b$	Q^a	ref
TTF	1.349	1.757	0.768	0.133	26
TTF–TCNQ	1.369	1.743	0.785	0.480	27
TTF–ClO$_4$	1.404	1.713	0.820	1.194	28
TTF–HgCl$_3$	1.411	1.721	0.820	1.149	24c
TTF–Cl$_{0.67}$	1.381	1.720	0.803	0.847	29
4	1.373	1.727	0.795	0.684	this work

^{a} $Q = -15.55 + 20.42r$. From ref 25.

Table 4. Comparison of Various Parameters of **1**–**4**

distances	Phz (**1**)	Fe(Cp)$_2$ (**2**)	Fe(Cp*)$_2$ (**3**)	TTF (**4**)
hydrogen bond/Å	2.65	2.67	2.68	2.68
interlayer M–M/Å	14.57	9.79	13.13	13.45
intralayer M–M/Å	7.31	7.09	7.33	7.18
tilt angle/°	72.6	76.1	67.7	74.8
stacking (CA^{2-}–CA^{2-})/Å	3.58	3.54	3.44	3.56

Scheme 3

9.79 Å
13.13 Å
13.45 Å
14.57 Å
= {[Fe(CA)$_2$(H$_2$O)$_2$]$^{m-}$}$_l$ Layer
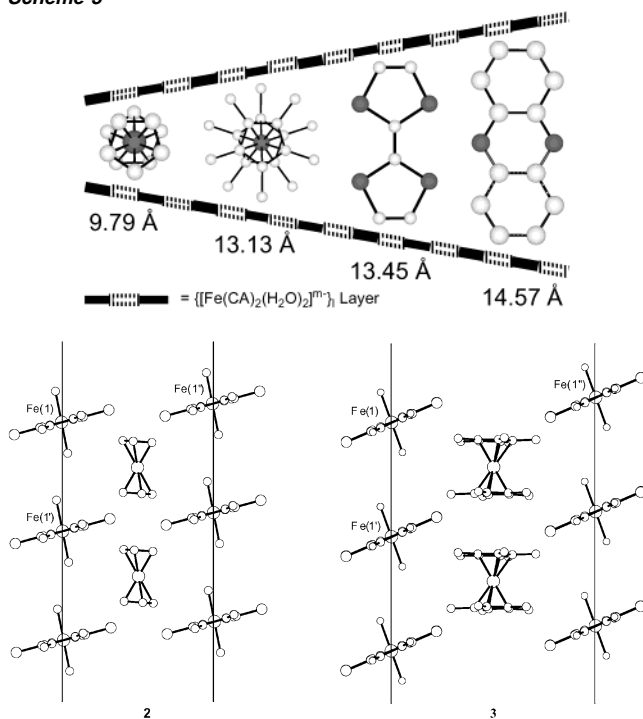
Figure 3. Tilt angles between the chloranilate planes and the metal connecting planes; 76.1° for **2** (left) and 67.7° for **3** (right).

in the structures of **2** and **3**. Hydrogen-bonding distance of **3** between the monomers (2.68 Å) is similar to that of **2** (2.67 Å). However, tilt angles between the chloranilate planes and the metal connecting planes of the layer are 76.1° for **2** and 67.7° for **3**, respectively (Figure 3). Chlorine atoms play two types of roles (Scheme 4): (i) making channels between the layers and (ii) sensing the guests and reforming the layer structure by changing their tilt angles and stacking distances according to their sizes and shapes.

Physical Properties. Raman and Electronic Spectroscopy. Raman spectroscopy is used as a rapid means of determining the charge on the TTF molecule by comparing the ν_2 and ν_3 modes of symmetrical central C=C bond in the range 1385–

Scheme 4. Structural Parameters for Well-Suited Intercalated Structure
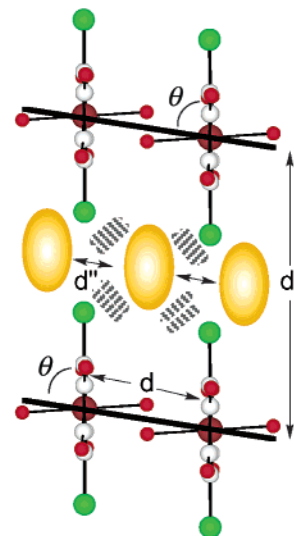
1540 cm^{-1}.[30] Raman spectrum of **4** (Supplementary Figure S5) shows a weak peak at 1516 cm^{-1} (ν_2) and a strong peak at 1445 cm^{-1} (ν_3). The formal charge of TTF molecule in **4** estimated from these frequencies is 0.75+, which is very similar to that of mixed-valence TTF halide.[30c] The value well agrees with the one calculated using the C–S and C=C bond lengths and the stoichiometry of **4**. The electronic spectrum of **4** shows peaks at 5000 and 12900 cm^{-1} (Supplementary Figure S6). These peaks are typical of charge-transfer bands for conducting compounds and are characteristics of a mixed-valence state which support the above Raman spectrum data.[24a,31,32]

Mössbauer Spectroscopy. The ^{57}Fe Mössbauer spectra for compounds **1** and **3** at 205 and 78 K and **4** at 297, 205, and 78 K are shown in Figure 4a, 4b, and 4c, respectively. The spectra of **1** are fitted with a one quadrupole-split doublet: an isomer shift (IS) = 0.45 mm s^{-1} and quadrupole splitting (QS) = 1.35 mm·s^{-1} at 205 K, and IS = 0.51 mm·s^{-1} and QS = 1.32 mm·s^{-1} at 78 K. These parameters indicate that [Fe(CA)$_2$(H$_2$O)$_2$]$^{m-}$ anion in **1** is consistent with high-spin (S = 5/2) iron(III) ions.[33,34]

The spectrum of **3** consists of one singlet (IS = 0.50 mm·s^{-1} at 205 K and IS = 0.54 mm·s^{-1} at 78 K) and one doublet (IS = 0.47 mm·s^{-1} and QS = 1.42 mm·s^{-1} at 205 K and IS = 0.51 mm·s^{-1} and QS = 1.39 mm·s^{-1} at 78 K). The doublet

(26) Cooper, W. F.; Kenny, N. C.; Edmonds, J. N.; Nagel, A.; Wudl, F.; Coppens, P. *Chem. Commun.* **1971**, 889. *9*, 36.
(27) Kistenmacher, T. J.; Phillips, T. E.; Cowan, D. O. *Acta Crystallog.* **1974**, *B30*, 763.
(28) Yakushi, K.; Nishimura, S.; Sugano, T.; Kuroda, H.; Ikemoto, I. *Acta Crystallogr.* **1980**, *B36*, 358.
(29) Williams, R.; Ma, C. L.; Samson, S.; Khanna, S. K.; Somoanao, R. B. *J. Chem. Phys.* **1980**, *72*, 3781.
(30) (a) Duyne, R. P. V.; Cape, T. W.; Suchanski, M. R.; Siedle, A. R. *J. Phys. Chem.* **1986**, *90*, 739. (b) Temkin, H.; Fitchen, D. B.; Wudl, F. *Solid State Commun.* **1977**, *24*, 87. (c) Matsuzaki, S.; Moriyama, T.; Toyoda, K. *Solid State Commun.* **1980**, *34*, 857.
(31) (a) Scott, B. A.; Placa, S. J. L.; Torrance, J. B.; Silverman, B. D.; Welber, B. *J. Am. Chem. Soc.* **1977**, *99*, 6631. (b) Triki, S.; Ouahab, L.; Halet, J.; Peña, O.; Padiou, J.; Grandjean, D.; Garrigou-Lagrange, C.; Delhaes, P. *J. Chem. Soc., Dalton Trans.* **1992**, 1217. (c) Miyazaki, T.; Matsuzaki, S.; Ichimura, K.; Sano, M. *Solid State Commun.* **1993**, *85*, 949.
(32) The polycrystalline-pellet dc electrical conductivity measured by standard four-probe technique between 300 and 130 K for **4** is 2.6 × 10^{-3} S·cm^{-1} at R. T. and 1.9 × 10^{-5} S·cm^{-1} at 130 K. (Suplementary Figure S9). It behaves as a semiconductor with high activation energy, 0.19 eV.
(33) (a) Dickson, D. P. E.; Berry, F. J. *Mössbauer Spectroscopy*; Cambridge University Press: Cambridge, U.K., **1986**. (b) Grillo, V. A.; Hanson, G. R.; Wang, D.; Hambley, T. W.; Gahan, L. R.; Murray, K. S.; Moubaraki, B.; Hawkins, C. J. *Inorg. Chem.* **1996**, *35*, 3568.
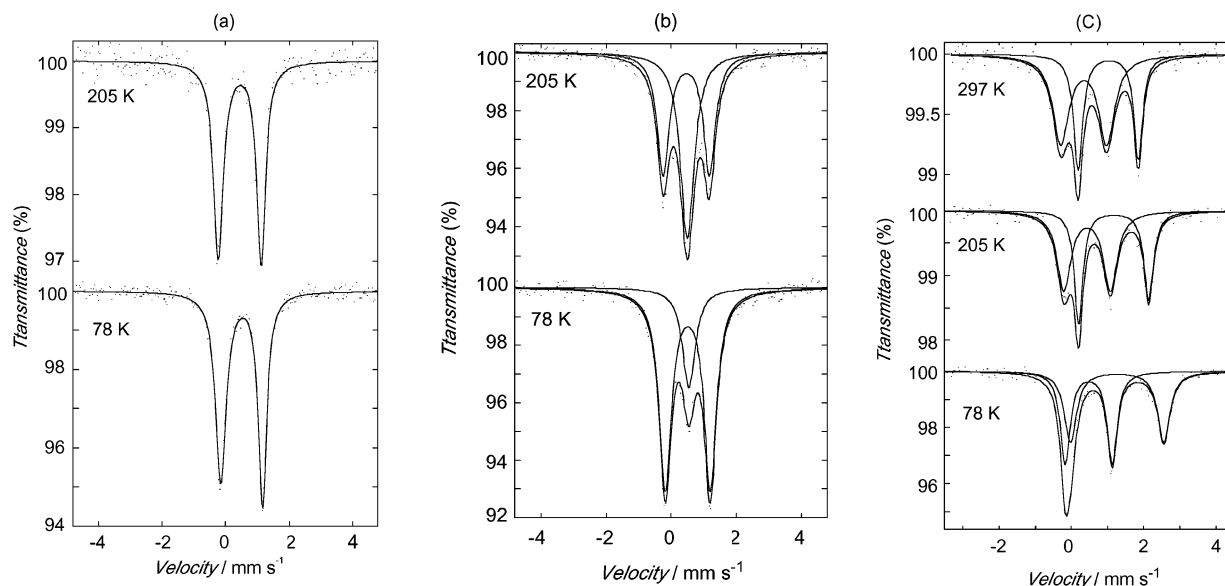
Figure 4. (a) ^{57}Fe Mössbauer spectra of **1**, (b) ^{57}Fe Mössbauer spectra of **3** showing the overlap of one singlet and one quadrupole doublet typical of low-spin iron(III) and high-spin iron(III), and (c) ^{57}Fe Mössbauer spectra of **4**.

absorption is similar to that of **1**, confirming the existence of high-spin iron(III) ions in **3**. The value of the *IS* for the singlet absorption is characteristic of the $[Fe(Cp^*)_2]^+$ in the $S = 1/2$ ground doublet of low-spin iron(III) ions.[21,35] The spectral feature of **3** is also similar to that of **2** ($IS = 0.43$ mm·s^{-1} for the singlet and $IS = 0.40$ mm·s^{-1} and $QS = 1.38$ mm·s^{-1} for the doublet).[15c] The area ratio of Fe^{3+}_{LS}:Fe^{3+}_{HS} signals at 205 K is 0.95, which is in good agreement with the ratio expected from the stoichiometry of **3**. However, the intensity of singlet absorption corresponding to $[Fe(Cp^*)_2]^+$ cation at 78 K becomes weaker: the ratio decreases to 0.28. Such phenomenon along with the absorption broadening with decreasing temperature is observed in the similar structural compound $\{[Fe(Cp^*)_2]\text{-}[C_3(C(CN)_2)_3]\}_n$, suggesting that the columnar structure of the $[Fe(Cp^*)_2]^+$ cation may influence the electronic property of the iron(III) ion.[35a,36]

In the spectra of **4**, two quadrupole-split doublets are observed at 297, 205, and 78 K, which correspond to high-spin iron(II) ions ($IS = 1.10$ mm·s^{-1} and $QS = 1.66$ mm·s^{-1} at 297 K, $IS = 1.17$ mm·s^{-1} and $QS = 1.94$ mm·s^{-1} at 205 K, $IS = 1.27$ mm·s^{-1} and $QS = 2.58$ mm·s^{-1} at 78 K) and high-spin iron-(III) ions ($IS = 0.42$ mm·s^{-1} and $QS = 1.27$ mm·s^{-1} at 297 K, $IS = 0.44$ mm·s^{-1} and $QS = 1.28$ mm·s^{-1} at 205 K, $IS = 0.48$ mm·s^{-1} and $QS = 1.30$ mm·s^{-1} at 78 K), respectively.[37] Observation of these two doublets at 297, 205, and 78 K in **4** evidently indicates that the anionic layer of iron-chloranilate is

a valence-trapped mixed-valence electronic state, where the electron-transfer rate between the two iron species is less than the Mössbauer time scale.[38] The *IS* and *QS* values for the two doublets in the spectrum of **4** decrease as the temperature is increased. These changes are normal and do not reflect the onset of intermolecular electron transfer. The decrease in *IS* values with increasing temperature is due to the second-order Doppler shift.[38a,39] In the high-spin iron(II) ions, the temperature dependence seen in *QS* values results from the change in the thermal population of low-lying excited states which result from the spin−orbit splitting of the $^5T_2$ state.[14] The area ratio of Fe^{2+}: Fe^{3+} absorption is 0.97 at 78 K and decreases slightly to 0.81 at 297 K, which is consistent with a somewhat higher recoil-free fraction expected for the ferric site. This ratio indicates the existence of Fe^{2+} and Fe^{3+} in the ratio of 1:1, and the formal oxidation state of iron ion in $[Fe(CA)_2(H_2O)_2]^{m-}$ is 2.5+. This is in good agreement with our assumption from the TTF charge and the averaged Fe−O bond distances, which are intermediate between $Fe^{2+}-$O and $Fe^{3+}-$O. However, two kinds of iron species in **4** cannot be observed by X-ray measurement, although X-ray time scale is larger than Mössbauer time scale. This is attributed to the space group symmetry or the random super-position of Fe^{2+} and Fe^{3+} in the crystal lattice.[38b,40]

The common feature of the Mössbauer spectra in **1**, **2**, and **3** is that the values of *IS* and *QS* of high-spin iron(III) are very similar. These compounds are constructed from the common layers, which consist of the same building blocks of $[Fe^{3+}(CA)_2\text{-}(H_2O)_2]^-$. On the other hand, the Mössbauer spectra of **4** indicate that the mixed-valence layers in **4** consisting of the iron(II)- and iron(III)-chloranilate monomers introduce and stabilize the mixed-valence state of $TTF^{0.75+}$ in-between.

(34) The temperature dependence of the recoil-free fraction, ln[A(T)/A(78)] of **1** (Supplementary, Figure S7) shows a nonlinearity above 250 K indicative of the existence of a phase transition. This situation is well supported by the DSC traces of **1**, which shows one thermal anomaly at 270 K (Supplementary, Figure S8). The origin of the phase transition is not clear at this stage. However, protons of water molecules may moderate the phase transition and cause the inflection of Mössbauer spectral intensities at around 250 K through hydrogen-bonding interaction.

(35) (a) Miller, J. S.; Calabrese, J. C.; Rommelmann, H.; Chittipeddi, S. R.; Zhang, J. H.; Reiff, W. M.; Epstein, A. J. *J. Am. Chem. Soc.* **1987**, *109*, 769. (b) Miller, J. S.; Ward, M. D.; Zhang, J. H.; Reiff, W. M. *Inorg. Chem.* **1990**, *29*, 4063. (c) Miller, J. S.; Zhang, J. H.; Reiff, W. M. *J. Am. Chem. Soc.* **1987**, *109*, 4584.

(36) (a) Miller, J. S.; Epstein, A. J.; Reiff, W. M. *Acc. Chem. Res.* **1988**, *21*, 114. (b) Miller, J. S.; Krusic, P. J.; Dixson, D. A.; Reiff, W. M.; Zhang, J. H.; Anderson, E. C.; Epstein, A. J. *J. Am. Chem. Soc.* **1986**, *108*, 4459. (c) Yee, G. T.; Whitton, M. J.; Sommer, R. D.; Frommen, C. M.; Reif, w. M. *Inorg. Chem.* **2000**, *39*, 1874.

(37) Greenwood, N. N.; Gibb, T. C. *Mössbauer Spectroscopy*; Chapman and Hall: London, 1982.

(38) (a) Oh, S. M.; Wilson, S. R.; Hendrickson, D. N.; Woehler, S. E.; Wittebort, R. J.; Inniss, D.; Strouse, C. E. *J. Am. Chem. Soc.* **1987**, *109*, 1073. (b) Manago, T.; Hayami, S.; Oshio, H.; Osaki, S.; Hasuyama, H.; Herber, R. H.; Maeda, Y. *J. Chem. Soc., Dalton Trans.* **1999**, 1001.

(39) Sugiura, Y.; Tanaka, H.; Mino, Y.; Ishida, T.; Ota, N.; Inoue, M.; Nomoto, K.; Yoshioka, H.; Takemoto, T. *J. Am. Chem. Soc.* **1981**, *103*, 6979.

(40) DeBord, J. R. D.; Reiff, W. M.; Warren, C. J.; Haushalter, R. C.; Zubieta, J. *Chem. Mater.* **1997**, *9*, 1994.
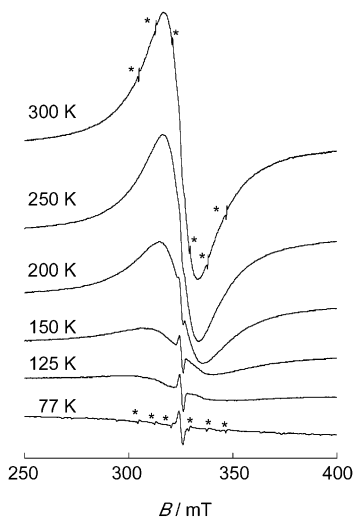
Figure 5. Temperature dependence of EPR spectra for **4** ($\nu = 9.126$ GHz) (signals of standard MnO are labeled with asterisks).

Electron Paramagnetic Resonance. At the temperature range of 77−300 K, the compound **1** is EPR silent. This indicates that the phenazine in **1** is not in radical form $(phz^{+0.5})_2$ as reported earlier;[15b] rather, the proton on phz is disordered between two phz molecules, that is, $(H_{0.5}phz)_2$. At the temperature range of 77−300 K, the compounds **2** and **3** are also EPR silent, probably because of the short spin−lattice relaxation T_1 and the short spin−spin relaxation T_2 caused by the intralayer exchange interaction of $[Fe(Cp)_2]^+$ (**2**) and $[Fe(Cp^*)_2]^+$ (**3**).[41]

EPR spectra of a polycrystalline sample of **4** at selected temperatures are shown in Figure 5. The spectrum at 300 K consists of two types of signals: a weak and sharp one (a) and a strong and broad one (b). The value of g for both the signals is 2.008, which is attributed to TTF radicals. The temperature dependence of the integrated intensity of two signals in the range of 77−300 K are completely different. The intensity of signal a is unchanged upon decreasing temperature, which is attributed to a Pauli type paramagnetism, typical of metallic and highly conducting radical salts.[32,42] The intensity of signal b drastically decreases with decreasing temperature and completely disappears at 77 K. This phenomenon may be due to antiferromagnetic spin−spin interactions between the neighboring TTF radicals in the columns. This is also identified with the magnetic behavior above 100 K (vide infra).[43]

Magnetic Properties. The temperature dependence of magnetic susceptibilities (χ) of compounds **1**−**4** are measured over temperature range of 2−300 K in applied field of 0.5 T. The variation of $\chi_m T$ versus T for all the compounds are plotted in Figure 6. The values of $\chi_m T$ in the compounds **1**, **2**, and **3** decrease slightly with decreasing temperature and at lower temperature they decrease rapidly, indicative of the existence of weak antiferromagnetic interaction. The value of $\chi_m T$ at 300 K for **1** is 4.29 emu·mol^{-1}·K. This value agrees with the presence of a magnetically isolated high-spin ($S = 5/2$) iron-(III) ion. The magnetic susceptibility data for **1** are least-squares
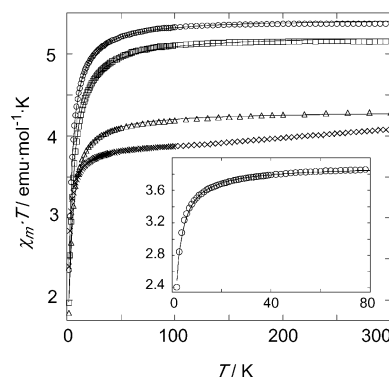
(41) Golhen, S.; Ouahab, L.; Grandjean, D.; Molinie, P. *Inorg. Chem.* **1998**, *37*, 1499.
(42) Clemente-León, M.; Coronado, E.; Galan-Mascarós, J. R.; Giménez-Saiz, C.; Gómez-García, C. J.; Ribera, E.; Vidal-Gancedo, J.; Rovira, C.; Candell, E.; Laukhin, V. *Inorg. Chem.* **2001**, *40*, 3526.
(43) Geiser, U.; Wang, H. H.; Schlueter, J.; Chen, M. Y.; Kini, A. M.; Kao, I. H.; Williams, J. M.; Whangbo, M.; Evain, M. *Inorg. Chem.* **1988**, *27*, 4284.

Figure 6. Plots of the product of the molar susceptibility times the temperature versus temperature for **1** (open triangles), **2** (open squares), **3** (open circles), and **4** (cross marks). Inset, magnetic susceptibility of **4** below 80 K. Solid lines are theoretical fits of the data with the parameters listed in the text.

fitted to the quadratic layer equation (χ_{2D}) for isotropic intralayer antiferromagnetic exchange among the nearest-neighbor $[Fe(CA)_2(H_2O)_2]^-$ monomers through the intralayer hydrogen bonding and stacking interaction (eq 1).[44]

$$\chi_{2D} = \frac{Ng_{2D}^2\mu_B^2}{2J_{2D}}\left(3\theta + \frac{4}{\theta^0} + \frac{1.448}{\theta^1} + \frac{0.228}{\theta^2} + \frac{0.262}{\theta^3} + \frac{0.119}{\theta^4} + \frac{0.017}{\theta^5} + ...\right)^{-1} \quad (1)$$

$$\theta = kT/2J_{2D}\cdot S(S + 1) \quad (2)$$

A good simulation of the magnetic susceptibility is achieved with $g_{2D} = 2.003$, $J_{2D} = -0.071$ cm^{-1} as indicated by the solid curve in Figure 6.

For compounds **2** and **3**, $\chi_m T$ values at 300 K are 5.15 and 5.37 emu·mol^{-1}·K, respectively. These values are attributed to the presence of two magnetically independent high-spin ($S = 5/2$) iron(III) ions for $[Fe(CA)_2(H_2O)_2]^-$ and low-spin ($S = 1/2$) iron(III) ions for $[Fe(Cp)_2]^+$ (**2**) and $[Fe(Cp^*)_2]^+$ (**3**), while the values are larger than the sum of the spin only values of the $S = 5/2$ and $S = 1/2$ (4.76 emu·K·mol^{-1}) due to significant orbital contributions of $[Fe(Cp)_2]^+$ and $[Fe(Cp^*)_2]^+$. The magnetic susceptibility data (χ_{total}) for **2** and **3** are least-squares fitted to the sum of the quadratic-layer equation (χ_{2D}) for isotropic antiferromagnetic exchange among the nearest-neighbor $[Fe(CA)_2(H_2O)_2]^-$ monomers and the Heisenberg antiferromagnetic linear chain equation (χ_{1D}) for the intrachain stacking interaction in one-dimensional arrays of $[Fe(Cp)_2]^+$ (**2**) and $[Fe(Cp^*)_2]^+$ (**3**) (eq 3):[45]

$$\chi_{total} = \chi_{2D} + \chi_{1D} \quad (3)$$

$$\chi_{1D} = \frac{Ng_{1D}^2\mu_B^2}{kT} \frac{0.25 + 0.074975x + 0.075235x^2}{1.0 + 0.9931x + 0.172135x^2 + 0.757825x^3} \quad (4)$$

$$x = |2J_{1D}|/kT \quad (5)$$

A good simulation of the magnetic susceptibility is achieved with $g_{2D} = 2.008$, $J_{2D} = -0.089$ cm^{-1}, $g_{1D} = 3.132$, $J_{1D} =$

(44) Lines, M. E. *J. Phys. Chem. Solids* **1970**, *31*, 101.
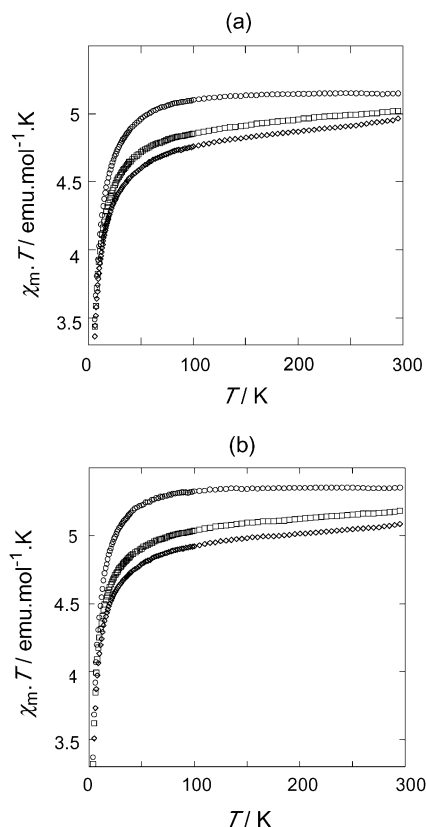(45) Bonner, J. C.; Fisher, M. E. *Phys. Rev.* **1964**, *A135*, 640.

Figure 7. Plots of the product of the molar susceptibility times the temperature versus temperature for **2** (a) and **3** (b): $B = 0.5$ T (open circles); $B = 0.05$ T (open squares); $B = 0.005$ T (open rhombuses).

-1.657 cm^{-1} for **2** and $g_{2D} = 2.006$, $J_{2D} = -0.066$ cm^{-1}, $g_{1D} = 3.440$, $J_{1D} = -1.287$ cm^{-1} for **3**, as indicated by the solid curve in Figure 6. The observed anisotropic g_{1D}-factor of [Fe(Cp)$_2$]$^+$ (**2**) and [Fe(Cp*)$_2$]$^+$ (**3**) are higher than the expected values, $g = 2.71$ for [Fe(Cp)$_2$]$^+$ and $g = 2.79$ for [Fe(Cp*)$_2$]$^+$.[46] However, the obtained g_{1D}-factors agree well with the magnetic and EPR data of other ferrocenium derivatives and appear to be consistent with the significant orbital contributions from the ^{2}E ground state to the magnetic moment.[35a,36c,47]

To confirm the origin of the large $\chi_m T$ values in the compounds **2** and **3**, the temperature dependence of magnetic susceptibilities (χ) is measured over the temperature range of 2−300 K in applied field of 0.05 and 0.005 T (Figure 7). In both compounds, the temperature-dependent behavior at 0.05 and 0.005 T are similar to that of 0.5 T. However, the value of $\chi_m T$ at 300 K is lower than those at 0.5 T: 5.03 emu·mol^{-1}·K at 0.05 T and 4.97 emu·mol^{-1}·K at 0.005 T for **2**, and 5.18 emu·mol^{-1}·K at 0.05 T and 5.09 emu·mol^{-1}·K at 0.005 T for **3**. Similar phenomenon is observed in the compound {[Fe(Cp*)$_2$][C$_3$(C(CN)$_2$)$_3$]}$_n$, which exhibits a field-induced phase transformation.[35a] The magnetic field dependent behavior is not observed in **1**. These peculiar behaviors of intrachain coupling in the one-dimensional columnar structure of [Fe(Cp)$_2$]$^+$ (**2**) and [Fe(Cp*)$_2$]$^+$ (**3**) are induced by the iron-chloranilate layer, which afford the space of the one-dimensional columns of guests.

For compound **4**, the temperature dependence of magnetic susceptibility also indicates the existence of antiferromagnetic interaction. The $\chi_m T$ value (4.08 emu·mol^{-1}·K) at 300 K is slightly lower than that of **1** reflecting the presence of a valence-trapped mixed-valence state of high-spin ($S = 5/2$) iron(III) ions and high-spin ($S = 2$) iron(II) ions. Although the temperature dependence of magnetic susceptibility for **4** is similar to that of **1**, **2**, and **3** below 80 K, the $\chi_m T$ value decreases faster than the others with decreasing temperature in the range of 300−80 K, indicating that antiferromagnetic interaction of **4** at high-temperature range is larger than those of **1**, **2**, and **3**. From this behavior, it is assumed that antiferromagnetic interactions at high temperature may be induced by the localized spins of mixed-valence TTF radical cations of one-dimensional column.[48] Therefore, the magnetic susceptibility data (χ_{Fe}) below 80 K can be fitted to the quadratic-layer equation for isotropic intralayer antiferromagnetic exchange among the nearest-neighbor mixed-valence states of iron(III)- and iron(II)-chloranilate monomers (1:1) through the intralayer hydrogen bonding and stacking interaction (eq 6):

$$\chi_{Fe} = 1/2\chi_{Fe(II)} + 1/2\chi_{Fe(III)} \tag{6}$$

where $\chi_{Fe(II)}$ and $\chi_{Fe(III)}$ are the molar magnetic susceptibility of iron(II) and iron(III), respectively. A good simulation of the magnetic susceptibility is achieved with $g_{Fe(III)} = 2.004$, $g_{Fe(II)} = 2.148$, and $J = -0.045$ cm^{-1} (Figure 6). These parameters are used to calculate the difference between the observed and calculated values above 80 K to obtain the contribution from the TTF radical cations (eq 7):[49]

$$\chi_{TTF} = \chi_{total} - \chi_{Fe} \tag{7}$$

The resulting difference (χ_{TTF}) and the normalized intensity ratio ($I(T)/I(300)$) of EPR signals are plotted versus temperature as shown in Figure 8. The similarity of both the plots demonstrates that spin−spin interaction between the neighboring TTF radical cations results in strong antiferromagnetic interaction directed to one-dimensional columnar structure at high-temperature range. χ_{TTF} is least-squares fitted to the Heisenberg alternating antiferromagnetic linear chain equation for isotropic exchange in the one-dimensional array of TTF cations through the two types of intrachain stacking interactions (eq 8).[16,50]

$$\chi_{TTF} = n_s \cdot \chi_{1Dalt} \tag{8}$$

$$\chi_{1Dalt} = \frac{Ng_{1D}^2\mu_B^2}{kT} \cdot \frac{A + Bx + Cx^2}{1.0 + Dx + Ex^2 + Fx^3} \tag{9}$$

$$x = |2J_{1D}|/kT \tag{10}$$

In the above equations, n_s is the number of spins per unit cell and α[51] is the alternation parameter. The fitting gives intrachain exchange interaction with $n_s = 1.38$, $J_{1D} = -308$ cm^{-1}, and α

(46) (a) Hendrickson, D. N.; Sohn, Y. S.; Gray, H. B. *Inorg. Chem.* **1971**, *10*, 1559. (b) Duggan, D. M.; Hendrickson, D. N. *Inorg. Chem.* **1975**, *14*, 955.

(47) Miller, J. S.; Calabrese, J. C.; Harlow, R. L.; Dixon, D. A.; Zhang, J. H.; Reiff, W. M.; Chittipeddi, S.; Selover, M. A.; Epstein, A. J. *J. Am. Chem. Soc.* **1990**, *112*, 5496.
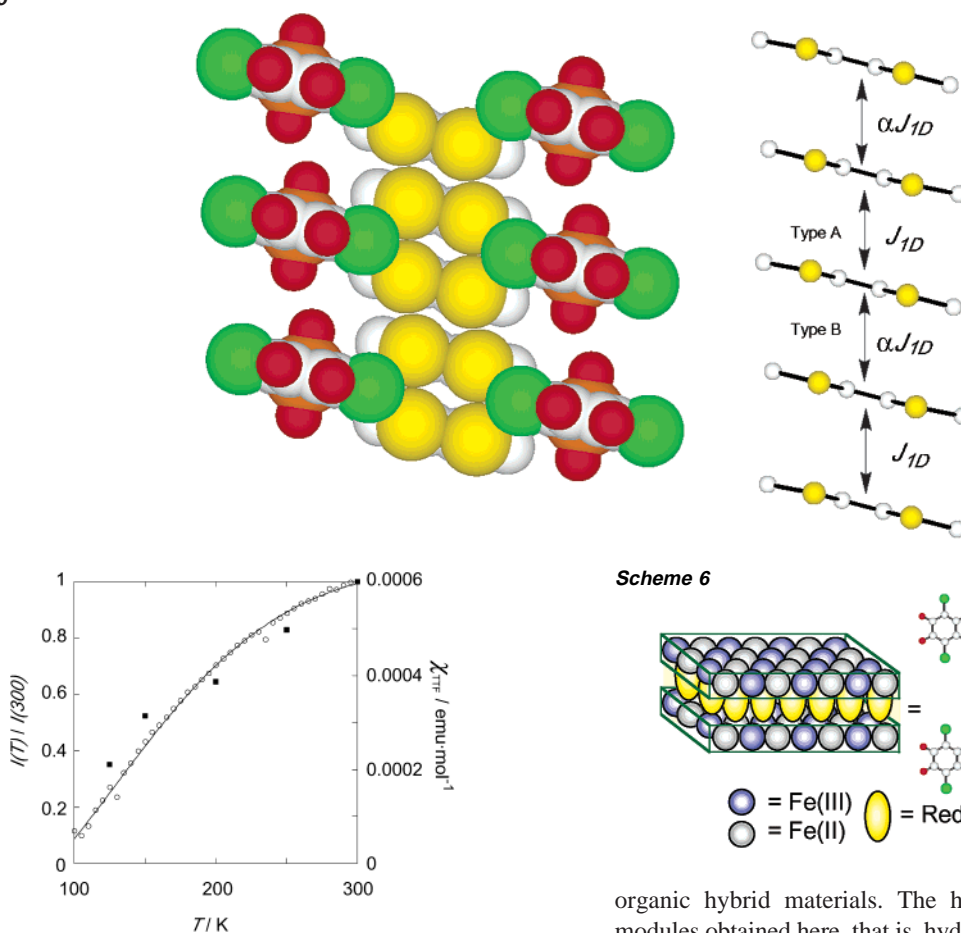
(48) (a) Rombaut, G.; Turner, S. S.; Pévelen, D. L.; Mathoniére, C.; Day, P.; Prout, K. *J. Chem. Soc., Dalton Trans.* **2001**, 3244. (b) Turner, S. S.; Pevelen, D. L.; Day, P.; Prout, K. *J. Chem. Soc., Dalton Trans.* **2000**, 2739. (c) Yoneyama, N.; Miyazaki, A.; Enoki, T.; Ogura, E.; Kuwatani, Y.; Iyoda, M. *Bull. Chem. Soc. Jpn.* **1999**, *72*, 2423. (d) Coronado, E.; Galan-Mascaros, J. R.; Gimenez-Saiz, C.; Gomez-Garcia, C. J.; Triki, S. *J. Am. Chem. Soc.* **1998**, *120*, 4671.

(49) Kurmoo, M.; Day, P.; Guionneau, P.; Bavic, G.; Chasseau, D.; Ducasse, L.; Allan, M. L.; Marsden, I. D.; Friend, R. H. *Inorg. Chem.* **1996**, *35*, 4719.

(50) Hatfield, W. E. *J. Appl. Phys.* **1981**, *52*, 1985.

Scheme 5

Scheme 6

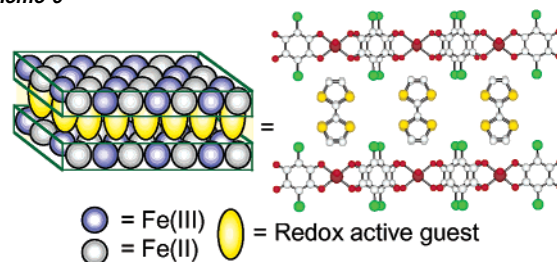⬤ = Fe(III)   ⬭ = Redox active guest
◯ = Fe(II)

Figure 8. Temperature dependence of the normalized EPR intensity (solid squares) and of the magnetic susceptibiliy of the TTF contribution (open circles). The solid line is theoretical fit.

$= 0.34$ in the temperature range of $100-300$ K, using the experimental value of g (2.008) from the EPR result. These results indicate that the antiferromagnetic interaction through the column dominates over the layer structure above 80 K. This is due to the spatial organization of the TTF cations leading to one-dimensional columnar network with rare S···S contacts. However, the values of J_{1D} and αJ_{1D} reflect two types of S···S stacking interactions (Scheme 5) and indicate that the exchange is stronger between the stacked TTF cations of smaller distances. This may be due to the presence of the anionic layer parallel to these stacks, which distribute its charge and affect the arrangement of the TTF ions of the column inducing the special magnetic properties.

Conclusion

In this study, it is shown how the hydrogen-bond-supported anionic layers based on iron-chloranilate mononuclear complexes can be used as inorganic hosts for the intercalation of guest cations to construct new types of multilayered inorganic–

(51) For $0 \leq \alpha \leq 0.4$, these coefficients are $A = 0.25$, $B = -0.062935 + 0.11376\alpha$, $C = 0.004778 - 0.033268\alpha + 0.12742\alpha^2 - 0.32918\alpha^3 + 0.25203\alpha^4$, $D = 0.053860 + 0.70960\alpha$, $E = -0.00071302 - 0.10587\alpha + 0.54883\alpha^2 - 0.20603\alpha^3$, $F = 0.047193 - 0.0083778\alpha + 0.87256\alpha^2 - 2.7098\alpha^3 + 1.9798\alpha^4$, and for $0.4 \leq \alpha \leq 1$, they are $A = 0.25$, $B = -0.068475 + 0.13194\alpha$, $C = 0.0042563 - 0.031670\alpha + 0.12278\alpha^2 - 0.29943\alpha^3 + 0.21814\alpha^4$, $D = 0.035255 + 0.65210\alpha$, $E = -0.00089418 - 0.10209\alpha + 0.87155\alpha^2 - 0.18472\alpha^3$, $F = 0.045230 - 0.0081910\alpha + 0.8323\alpha^2 - 2.6181\alpha^3 + 1.92813\alpha^4$.

organic hybrid materials. The host assemblies of common modules obtained here, that is, hydrogen-bond-supported layers, $\{[Fe(CA)_2(H_2O)_2]^{m-}\}_1$, are so flexible that they can include and stabilize various kinds of guests in the channels. The mixed valence state of the compound **4** indicates that the layer is able to modify the arrangement of modules and control the charge by changing the ratio of iron(III) and iron(II) for the inclusion of guests, which have the various geometry and oxidation states (Scheme 6). Moreover, in all of the compounds, the guest ions stack to make one-dimensional columnar structure in the channels. Although the observed susceptibility of **2**, **3**, and **4** are the sum of contributions from the guest and host moieties and there is no measurable exchange between the two spin sublattices, magnetic-field dependent susceptibility (**2**, **3**) and strong antiferromagnetic coupling at high-temperature range around 300 K (**4**) are observed. These peculiar magnetic behaviors are induced by intrachain coupling in the one-dimensional columnar structure of guests. Therefore, the host layers include the guests to make one-dimensional columnar arrangement and induce physical property characteristics of these arrays.

The above results show that the present approach is a successful procedure to prepare new types of inorganic–organic hybrid materials with multi-functionalities. From this study, it is known that the hybrid materials incorporate functionality from both their inorganic and organic components but the design of molecular materials combining two or more cooperative properties remains a challenge. The advance in the design of molecular hybrids will depend on the crystal engineering that involves the development of convenient synthetic strategies leading to a better control of the supramolecular structure of the materials.

Supporting Information Available: Figures S1−S9, repre-senting Powder XRD diagrams of **1**, **2**, **3**, and **4**, Raman spectrum of **4**, UV−vis−NIR spectrum of **4**, recoil-free fraction, ln[A(T)/A(78)] of **1**, DSC traces of **1**, and electric conductivity plot of **4**, respectively; Tables S1−S2, representing atomic coordinates and equivalent isotropic displacement cofficients for **3** and **4** and bond distances (Å) and angles (°) of **3** and **4**; an X-ray crystallographic file (CIF). This material is available free of charge via the Internet at http://pubs.acs.org.

JA027895V